

# DIABETIC RETINOPATHY SCREENING USING CUSTOM-DESIGNED CONVOLUTIONAL NEURAL NETWORK

Fahman Saeed, Muhammad Hussain, Senior Member, IEEE, Hatim A Aboalsamh, Senior Member, IEEE, Fadwa Al Adel, Adi Mohammed Al Owaifeer

**Abstract—** The prevalence of diabetic retinopathy (DR) has reached 34.6% worldwide and is a major cause of blindness among middle-aged diabetic patients. Regular DR screening using fundus photography helps detect its complications and prevent its progression to advanced levels. As manual screening is time-consuming and subjective, machine learning (ML) and deep learning (DL) have been employed to aid graders. However, the existing CNN-based methods use either pre-trained CNN models or a brute force approach to design new CNN models, which are not customized to the complexity of fundus images. To overcome this issue, we introduce an approach for custom-design of CNN models, whose architectures are adapted to the structural patterns of fundus images and better represent the DR-relevant features. It takes the leverage of k-medoid clustering, principal component analysis (PCA), and inter-class and intra-class variations to automatically determine the depth and width of a CNN model. The designed models are lightweight, adapted to the internal structures of fundus images, and encode the discriminative patterns of DR lesions. The technique is validated on a local dataset from King Saud University Medical City, Saudi Arabia, and two challenging benchmark datasets from Kaggle: EyePACS and APTOS2019. The custom-designed models outperform the famous pre-trained CNN models like ResNet152, Densnet121, and ResNeSt50 with a significant decrease in the number of parameters and compete well with the state-of-the-art CNN-based DR screening methods. The proposed approach is helpful for DR screening under diverse clinical settings and referring the patients who may need further assessment and treatment to expert ophthalmologists.

**Index Terms—** Classification, Deep Learning, DeepPCANet, Diabetic retinopathy, Medical imaging, PCA

## I. INTRODUCTION

Diabetes is a leading global health dilemma. One of its serious complications is diabetic retinopathy (DR), which has a prevalence of 34.6% worldwide and is considered a primary cause of blindness among middle-aged diabetic patients [1, 2]. A patient has a high DR risk if he or she has diabetes for a long time or is poorly managed. The DR treatment at its early stage slows down the retinal microvascular degeneration process. Graders manually screen fundus images for detecting DR prognosis, which is time-consuming and subjective [3-5]. On the other hand, screening a large number of diabetic patients for the possible prevalence of DR puts a heavy load on graders and reduces their efficiency. It necessitates intelligent systems for

DR screening, and many ML-based systems have been proposed that show good results on public data sets. However, their performance is not certain in real DR screening programs, where there are different ethnicities, and the retinal fundus images are captured using different cameras. These factors affect these systems' performance and remain a challenge in their widespread use [6].

Deep CNN has shown remarkable results in many applications [7-9] and has been employed for DR screening [2, 10, 11]. A CNN model usually involves a large number of parameters and needs a large amount of data for training. A brute force approach, which has been widely used for DR screening, is to adopt a highly complex CNN model designed for object recognition and pre-trained on the ImageNet dataset, and fine-tune it using fundus images [12-14]. As the ImageNet dataset consists of natural images, and the structural patterns of natural images and fundus images are entirely different, the architectures of the fine-tuned models do not adequately encode the fundus images. In addition, the complexity of pre-trained models is very high and not customized to DR screening from fundus images.

Alternatively, CNN models are manually designed from scratch. The design process starts with a CONV layer of a small width (i.e., the number of filters) and increases the widths of CONV layers by a fixed ratio as the network goes deeper [12-14]. There is no way to know what should be the depth (i.e., the number of layers) of a CNN model; a hit-trial strategy is used to fix the depth. In addition, CNN models are trained using iterative optimization algorithms such as stochastic gradient descent algorithms, and their convergence heavily depends on the initial guess of learnable parameters. Different data-independent [15, 16] and data-dependent [17, 18] approaches have been proposed to initialize them.

The above discussion indicates that the development of a custom-designed lightweight CNN model for DR screening under diverse clinical settings is challenging; it entails answers to three design questions: (i) what must be the depth of the model, (ii) what must be the width of each of its convolutional (CONV) layer, i.e., the number of its kernels, and (iii) how to initialize the learnable parameters. To address these questions, we propose a constructive data-dependent approach for designing CNN models for DR screening under diverse clinical

settings that automatically determines the depth of the model, the width of each CONV layer and initializes the learnable parameters. A custom-designed model takes a fundus image as input and grades it into normal or DR levels. We validated the proposed approach on three datasets: a local DR dataset from King Saud University Medical City, Saudi Arabia, two benchmark Kaggle datasets: EyePACS [19] and APTOS2019 [20]. Specifically, the main contributions of the paper are as follows:

- We proposed a constructive data-dependent approach to design lightweight CNN models customized to DR screening under various clinical settings. It automatically determines the depth of the model, the width of each COVN layer and initializes the learnable parameters using the fundus images dataset.
- To corroborate the usefulness of the proposed approach, we applied it to build custom-designed lightweight CNN architectures for three datasets.
- We performed extensive experiments to show that the custom-designed lightweight CNN models compete well with the pre-trained models such as ResNet [13], DenseNet [14], and ResNeSt [21], and other state-of-the-art methods for DR screening.

The layout of the rest of the paper is as follows: the literature view is presented in Section II, datasets are described in Section III, the detail of the proposed method is given in Section IV, the detail of experiments and the results are presented in Section V, and finally, Section VI concludes the paper.

## II. PREVIOUS WORK

Different methods have been introduced for automatic DR screening; an extensive literature review is given in [22-24]. First, we provide an overview of the previous work on building a deep model and initializing its weights and then give an overview of the state-of-the-art techniques for DR diagnosis.

### A. Data-dependent deep models

Different researchers employed principal component analysis (PCA) in various ways to build deep networks. Chan et al. [25] created an unsupervised two-layer model (PCANet). It is not an end-to-end model and is used only for feature extraction. Philipp et al. [17] used PCA to re-initialize pre-trained CNN models to avoid vanishing or exploding gradient problems. Suau et al. [18] used PCA and correlation to compress the filters of pre-trained CNN models. Seuret et al. [26] employed PCA to initialize the layers of stacked auto-encoders (SAEs). The above PCA-based methods have been employed for designing a CNN-like model for feature extraction, data-dependent re-initialization of the pre-trained models, or compressing their weights to reduce their complexity, but not for the data-dependent design of end-to-end CNN models.

Zhong et al. [27] introduced a method to build a BlockQNN module automatically using the block-wise setup, Q-Learning paradigm and epsilon-greedy exploration, and stack them to get the automatic CNN model. They evaluated their method using CIFAR-10, CIFAR-100, and ImageNet. It needs a lot of computational resources. They used 32 GPUs and got the best

CNN model with BlockQNN after three days and Faster BlockQNN after 20 hours.

### B. DR Screening methods

Clinical DR screening categorizes a patient based on fundus images into different grades: level 0 (normal), level 1(mild), level 2 (moderate), level 3 (severe), and level 4 (proliferative). In the state-of-the-art on DR screening, various deep learning-based methods have been proposed, which address mainly three image-level DR grading scenarios: (i) SC1: normal and different levels of DR severity – a multi-class problem (ii) SC2: normal (level 0) vs. DR (levels 1~4) – a two-class problem, (iii) SC3: non-referral (level 0 and 1) vs. referral (levels 2-4) – a two-class problem. In the following paragraphs, we give an overview of the state-of-the-art best methods. Islam et al. [28] built a hand-designed CNN model consisting of 18 layers and 8.9 million learnable parameters. Its evaluation on the EyePACS dataset gave a sensitivity of 94.5%, a specificity of 90.2% for SC2, and a sensitivity of (98%) and a specificity of (94%) for SC3. Li et al. [29] introduced two hand-designed CNN models with 11 and 14 layers for feature extraction from the EyePACS dataset. The features from both models are fused and classified using an SVM classifier. They achieved an accuracy of 86.17% for SC1 and an accuracy of 91.05%, a sensitivity of 89.30%, and a specificity of 90.89% for SC2 using 5-fold cross-validation. Challa et al. [30] built a CNN model consisting of 10 layers for the EyePACS dataset and obtained an accuracy of 86% for SC1. Tymchenko et al. [31] built an ensemble of 20 CNN models. The ensemble used five versions of each of four pre-trained models: SE-ResNetXt50 with input sizes of 380x380 and 512x512, EfficientNet-B4, and EfficientNet-b5. It was fine-tuned using the APTOS2019 dataset. They got an accuracy of 91.9%, a sensitivity of 84%, specificity of 98.1%, and Kappa of 96.9% for SC1 on the APTOS2019 dataset. Sikder et al. [32] used an ensemble learning algorithm called ET classifier to classify the colored information of the fundus images from the APTOS2019 dataset. They filtered the dataset by removing many noisy samples and achieved an accuracy of 91% and a recall of 89.43% for SC1.

The above overview of the state-f-the-art methods shows that some methods used hand-designed CNN models and others employed pre-trained models and fine-tuning. For creating hand-designed models, the architectures of CNN models were fixed empirically using the hit-and-trial approach. In the case of fine-tuning, the complexity of the pre-trained models is very high and is not customized to the structures of fundus images.

## III. MATERIALS

We developed and validated custom-designed CNN models using two Kaggle challenge datasets: EyePACS [19] and APTOS2019 [20] and one local dataset collected at King Saud University Medical City (KSU-DR). Each dataset was preprocessed and augmented using the procedure described in Subsection 4.2.1. KSU-DR and EyePACS were divided into training (80%), validation (10%), and testing (10%). APTOS2019 consists of two sets: public training and public testing; 90% of the public training data was used for training,

and the remaining 10% for validation and public testing for testing.

#### A. KSU-DR

The data was collected after getting approval from the local Institutional Review Board committee of King Saud University Medical City. The samples were collected randomly from fundus images of diabetic patients acquired during their routine endocrinologist's appointment at the fundusoscopic screening clinic. Fundus images were captured with a non-mydratic fundus camera (3D-OCT-1-Maestro non-mydrasis fundus camera); a 45-degree fundus photo was captured from each eye. All patients were from Saudi Arabia, 44% were males, and 56% were females. The mean patient age was 53 years; 17% had type 1 diabetes, and 83% had type 2 diabetes. The mean duration of diabetes was 18 years (ranging from 4 - 42 years). Random samples of 1750 images were selected and graded by two expert ophthalmologists; 1024 were graded as normal, 477 as mild non-proliferative DR, 222 as moderate non-proliferative DR, 20 as severe non-proliferative DR, and 7 as proliferative DR (pdf).

#### B. EyePACS

EyePACS [19] consists of 88,702 color retinal fundus images with varying resolutions up to about 3000×2000 pixels [30], collected from 44,351 subjects, but only 35,126 labeled images are available in the public domain; most of the researchers used this set for the proposal of new algorithms [28, 33]. We also used 35,126 labeled images to design and evaluate the custom-designed CNN model. The images are graded into normal and 4 DR classes – mild, moderate, severe, and proliferative.

#### C. APTOS2019

APTOS2019 dataset [20] was published by the Asia Pacific Tele-Ophthalmology Society on the Kaggle competition website. Clinical experts graded the images into normal and 4 DR levels (mild, moderate, severe, and proliferative). The public domain version of this database contains 3662 fundus images for training and 1928 fundus images for testing.

### IV. PROPOSED METHOD

#### A. Problem Formulation

The problem is to predict whether a patient is normal or suffering from DR (with different levels of severity) using his/her retinal fundus images. Formally, let  $R^{h \times w \times 3}$  be the space of color retinal fundus images with resolution  $h \times w$  and  $P = \{1, 2, \dots, C\}$  be the set of labels where  $C$  is the number of classes, which represent different DR grades; in case of two grades (i.e., normal and DR),  $C = 2$ , such that  $c = 1$  means normal and  $c = 2$  stands for DR; when there are five grades,  $C = 5$ , and  $c = 1, 2, 3, 4, 5$  are the labels for normal, mild, moderate, severe, proliferative DR, respectively. To predict the grade of a patient, we need to define a mapping  $\phi: R^{h \times w \times 3} \rightarrow P$  that takes a fundus image  $\mathbf{x} \in R^{h \times w \times 3}$  and associates it to a label  $c \in P$ , i.e.  $\phi(\mathbf{x}) = c$ . We model the mapping function  $\phi$  using a custom-designed CNN model.

#### B. Custom-designed CNN model

The main constituent layer of a CNN model is the CONV layer, and the widely adopted CNN models contain a large number of CONV layers, e.g., VGGNet [34] contains 13 CONV layers. The number of layers (depth) and the number of filters in each layer (width) are fixed manually, keeping in view ImageNet challenge dataset [35], without following any formal procedure. Retinal fundus images have complex small-scale structures, which form discriminative patterns and are entirely different from those of the natural images in the ImageNet dataset. We design a CNN model for the DR problem by drawing its architecture from the fundus images; we determine the depth of a model and the widths of its CONV layers in a customized way using the discriminative information in fundus images specific to different DR levels. In this direction, the first design decision is about extracting discriminatory information. For this purpose, first, we select the most representative fundus images from the available DR dataset using the K-medoids clustering algorithm [36] and then apply PCA [37] to determine the widths of CONV layers and initialize them. The next design decision is about the depth (i.e., the number of CONV layers). We control the depth using the ratio of the between-class scatter matrix  $\mathbf{S}_b$  to the within-class scatter matrix  $\mathbf{S}_w$ . Finally, motivated by the design strategy of ResNet [13], we add global pooling layers that follow the last CONV layer, and their outputs are fused and fed directly to a softmax layer. These layers controls the drastic increase in the number of learnable parameters (which cause overfitting). The design process is worked out in detail and discussed in the following subsections, and its overview is shown in Figure 1.

##### 1) Preprocessing

The retinal fundus images are usually not calibrated and are surrounded by a black area, as shown in Fig 1(a). To center the retina and remove the black area around it, firstly, the retina circle is cropped, and the background is removed using the method presented in [32], and then it is resized to  $512 \times 512$  pixels. Usually, the DR datasets are imbalanced, i.e., the numbers of images of different classes are significantly different; we increase the data of minority classes using data augmentation. We apply affine transformations to randomly rotate the image with an angle  $\theta \in (-180, 180)$ .

##### 2) Selection of representative fundus images

We determine the widths of CONV layers using the most discriminative information embedded in fundus images. For this purpose, the most representative images are selected by clustering the training set. The discriminative features are extracted from fundus images to cluster the training set, and the algorithms like K-means [38] and K-medoids [36] can be employed. As the K-means algorithm yields the mean feature vectors as cluster centers, it is not suitable for selecting the representative fundus images. On the other hand, as the K-medoids algorithm selects the feature vectors as cluster centers, it is appropriate to choose the representative fundus images. We extract features from fundus images for clustering using the efficient LGDBP descriptor proposed in [39]. The extracted features are clustered using the K-medoids algorithm [36] into  $K$  clusters, and the fundus images corresponding to the centers

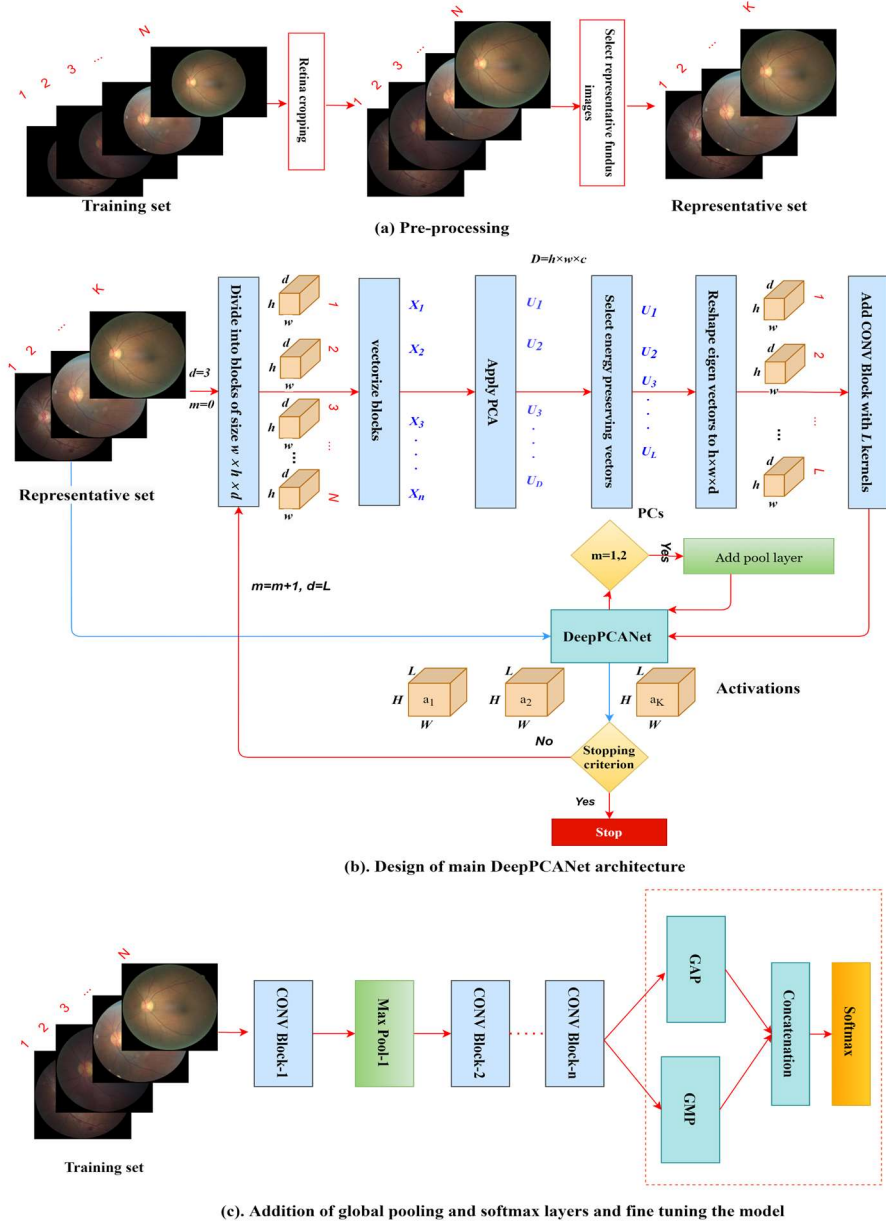


Fig 1. Design procedure of DeepPCANet

of the clusters are chosen as representative images. The number  $K$  of clusters is specified using the gap statistic method [40].

### 3) Designing the main DeepPCANet architecture

The design of the customized architecture of DeepPCANet needs to address the two questions, i.e., (i) what should be the depth of the model and (ii) what should be the width of each CONV layer. These questions are addressed by an iterative algorithm that incrementally adds CONV layers and stops when a specific criterion is satisfied. It is based on the idea of exploiting discriminative information of fundus images to select the number of kernels in a CONV layer and initialize them. It takes representative fundus images  $RI_j, j = 1, 2, 3, \dots, K$  as input divides them into patches of size  $7 \times 7$ . The patches are vectorized and used to determine the number of kernels and

initialize them. One possible idea is to cluster the patches and select the cluster centers as kernels, but the issue is choosing the number of clusters. We go for a simple and effective procedure, i.e., we employ PCA because it reduces the redundancy and causes to determine the kernels and their number, exploiting the discriminative information in the patches. The principal components (PCs), i.e., the eigenvectors along which the maximum energy is preserved, serve as kernels of the first layer. After computing the PCs, the DeepPCANet is initialized with an input layer and a CONV block (BN+RELU+CONV) with kernels equal to the number of PCs; the kernels are initialized by reshaping the PCs. Please note that we fix the size of patches to  $7 \times 7$  so that the size of kernels of the first CONV layers is  $7 \times 7$  following the convention of most of the existing CNN models



---

**Algorithm 2: To design the main DeepPCANet Architecture**


---

**Input:** Representative fundus images:  $RI_j, j = 1, 2, 3, \dots, K$  of size  $W \times H$  and the corresponding class labels  $c = 1, 2, \dots, C$ ; Energy threshold  $\varepsilon$

**Output:** The main architecture of DeepPCANet Architecture

---

**Processing**

**Step 1:** Initialize DeepPCANet with an input layer and set  $w = 7, h = 7, d = 3, m = 0$  (number of layers)

**Step 2:** Set  $a_j = RI_j, j = 1, 2, 3, \dots, K$  and  $TRP(\text{previous } TR) = 0$ .

**Step 3:** Divide  $a_j, j = 1, 2, 3, \dots, K$ , into blocks  $b_{ij}, i = 1, 2, 3, \dots, B, j = 1, 2, 3, \dots, K$ , of size  $w \times h \times d$ , where  $d$  is the number of channels (feature maps) in  $a_j$  and  $B$  is the number of blocks created from each  $a_j$ .

**Step 4:** Flatten  $b_{ij}$  into vectors  $\mathbf{x}_i \in R^D, i = 1, 2, \dots, M$ , where  $M = K \times B$ , and  $D = w \times h \times d$ .

**Step 5:** Compute zero-center vectors  $\phi_i, i = 1, 2, \dots, M$  such that  $\phi_i = \mathbf{x}_i - \bar{\mathbf{x}}$ , where  $\bar{\mathbf{x}} = \frac{1}{M} \sum_{i=1}^M \mathbf{x}_i$ .

**Step 6:** Compute the covariance matrix  $C = AA^T$ , where  $A = [\phi_1 \phi_2 \dots \phi_M]$ .

Calculate the eigenvalues  $\lambda_j$  and eigenvectors  $\mathbf{u}_j (j = 1, 2, \dots, D)$  of the covariance matrix  $C$ .

**Step 7:** Select  $L$  eigenvectors  $\mathbf{u}_i, i = 1, 2, \dots, L (L < D)$  corresponding to the  $L$  largest eigenvalues such that  $\frac{\sum_{l=1}^L \lambda_l}{\sum_{j=1}^D \lambda_j} \geq \varepsilon$ , where  $\varepsilon$  determines the level of energy to be preserved (e.g.  $\varepsilon = 0.99$ , for 99% energy preservation).

**Step 8:** All other eigenvectors corresponding to the  $\frac{\sum_{l=1}^L \lambda_l}{\sum_{j=1}^D \lambda_j} < \varepsilon$  are summation as one eigenvector and stacked to the  $L$  eigenvectors

**Step 9:** Reshape  $\mathbf{u}_i, i = 1, 2, \dots, L + 1$  to kernels of size  $W \times H \times D$ , and add the CONV block to DeepPCANet; Update  $m = m + 1$ .

**Step 10:** If  $m = 1$  or  $2$ , add a max pool layer with a pooling window of size  $2 \times 2$  and stride  $2$  to DeepPCANet.

**Step 11:** Compute the activations  $a_j, j = 1, 2, 3, \dots, K$  of representative fundus images  $RI_j, j = 1, 2, 3, \dots, K$  such that  $a_j = \text{DeepPCANet}(RI_j)$ .

**Step 12:** Compute the ratio  $TR = \frac{\text{Trace}(S_b)}{\text{Trace}(S_w)}$  where  $S_w = \sum_{i=1}^C \sum_{j=1}^{n_i} (x_j - \mu_i)(x_j - \mu_i)^T$  and  $S_b = \sum_{i=1}^C n_i (\mu_i - \mu)(\mu_i - \mu)^T$ .

**Step 13:** If  $TRP(\text{previous } TR) \leq TR$ , set  $TRP = TR, W = 3, H = 3, D = L$ , and go to Step 3, stop otherwise.

like Inception [12], ResNet [13], and DenseNet [14].

Using the current architecture of DeepPCANet, activations  $a_j, j = 1, 2, 3, \dots, K$  of representative images  $RI_j, j = 1, 2, 3, \dots, K$  are calculated. Inspired by the Fisher ratio [41], using these activations, the ratio of the trace ( $TR$ ) of between-class scatter matrix  $S_b$  to the trace of within-class scatter matrix  $S_w$  is calculated and is used to decide whether to stop or add another CONV block. The new CONV blocks continue to be added as long as  $TR$  continues to increase. This criterion ensures that the features generated by DeepPCANet have large inter-class variation and small intra-class scatter. To add a CONV block, the above procedure is repeated with activations  $a_j, j = 1, 2, 3, \dots, K$ . To reduce the size of feature maps for computational efficiency, pooling layers are added after the first and second CONV blocks. As the kernels and their number is determined from the fundus images, each layer can have a different number of filters. The detail of the design procedure is elaborated in Algorithm 2. It is to be noted that the PCs  $\mathbf{u}_i$ , which are used to specify the kernels of a CONV layer, are orthogonal and capture

most of the variability in input fundus images, without redundancy, in the form of independent features. The PCs are selected so that the maximum energy is preserved. The energy is measured in terms of the corresponding eigenvalues i.e.

$Energy = \frac{\sum_{l=1}^L \lambda_l}{\sum_{j=1}^D \lambda_j}$  [18, 42] and a threshold value is used to

ensure that a certain percentage of energy (e.g., 99%) is preserved. The threshold value of 99% preserves the maximum energy with 209 ( $L$ ) PCs for CONV1 in EyePACS dataset, as shown in Figure 2. The depth of a CNN model and the width of each layer are important factors determining the model complexity. Step 7 of Algorithm 2 adaptively determines the best number of kernels that ensure the preservation of maximum energy of the input image. Step 9 initializes the kernels to be suitable for the DR domain. The selected kernels extract the features from fundus images (5 classes) so that the variability of the structures in fundus images is maximally preserved. It is also essential that the features must be discriminative, i.e., have large inter-class variance and small intra-class scatter as we go deeper

in the network; it is ensured using the trace ratio  $TR = \frac{Trace(Sb)}{Trace(Sw)}$ , the larger the value of the trace ratio, the larger the inter-class variance, and the smaller the intra-class scatter [41]. Step 13 in Algorithm 2 allows adding CONV layers as long as  $TR$  increases and determines the data-dependent depth of DeepPCANet. As shown in Figure 4, the maximum ratio is at layers 4, 5, and 16 for KSU-DR, APTOS2019, and EyePACS, respectively. It means that the suitable depth of the DeepPCANet model for the KSU-DR dataset is four layers (Figure 4(a)), for APTOS2019 is five layers ((Figure 4(b)), and for EyePACS dataset is 16 layers ((Figure 4(c)). The model for EyePACS is deeper because it contains many poor-quality fundus images, and there is the possibility of label noise because only one expert graded each image in this dataset. Each dataset was collected from a different region and under different conditions using different cameras, so the architecture of the DeepPCANet model is different for each dataset.

#### 4) Addition of Global Pool and Softmax layers

The dimension of the activation of the last CONV block is  $W \times H \times L$ . If it is flattened and passed to an FC layer, the number of learnable weights and biases of the FC becomes excessively large, which leads to overfitting. To overcome this issue, the activation of the last CONV block is passed simultaneously to global average pooling (GAP), and global max-pooling (GMP) layers [43], which extract the mean and largest feature from each feature map, and these features are fused using a concatenation layer. Both GAP and GMP help reduce the number of learnable parameters and extract discriminative features from the activation. Finally, a softmax layer is introduced as a classification layer, and the output of the

concatenation layer is passed to this layer, as shown in Figure 1(c). A dropout layer is also added after the last CONV layer to overcome the overfitting problem.

#### 5) Finetuning the DeepPCANet Model

After determining the architecture of custom-designed DeepPCANet, it is fine-tuned using the training and validation sets. Fine-tuning involves various hyper-parameters: the optimization algorithm, learning rate, batch size, activation function, and dropout probability. We employed the Optuna optimization algorithm [44] to determine the best values of the hyperparameters. We tested three optimizers (Adam, SGD, and RMSprop), learning rate between  $1e-5$  and  $1e-1$ , four batch sizes (5, 10, 15, 20), three activation functions (Relu, LRelu, and Sigmoid), and dropout probability between 0.25 and 0.50. After training for ten epochs, the Optuna returned the best hyperparameters for each dataset, as shown in Table 1. The number of kernels in each layer of each model is based on an energy threshold of 0.99. The models for APTOS2019, KSU-

TABLE 1. THE BEST HYPERPARAMETERS FOUND USING OPTUNA ALGORITHM

Dataset	Activate function	learning rate	Patch's size	optimizer	dropout
KSU-DR	LRelu	0.0001	10	RMSprop	0.50
EyePACS	LRelu	0.0055	10	RMSprop	0.38
APTOS2019	LRelu	0.0007	5	RMSprop	0.40

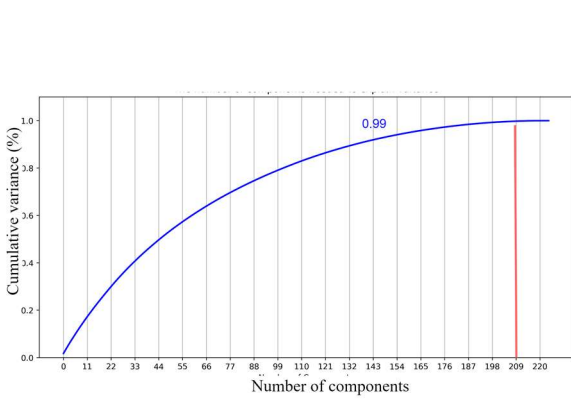


Fig. 2. Selecting the best threshold. The appropriate threshold is (0.99%) and the best number of eigenvectors is 209.

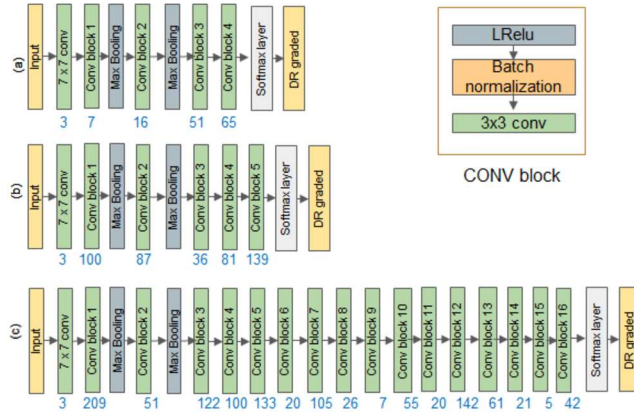


Fig. 3. DeepPCANet architecture for (a) APTOS (b) KSU-DR, and (c) EyePACS datasets

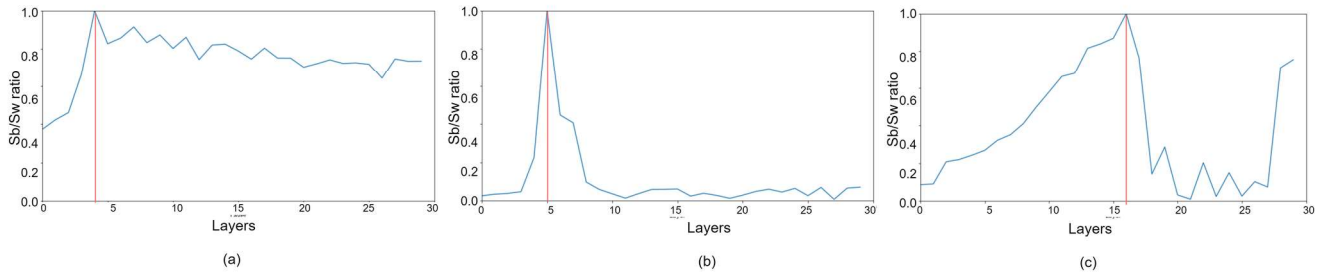


Fig. 4. Trace ratio of between class scatter and within class scatter. The depth for (a) APTOS2019 dataset is 4 layers, (b) KSU-DR dataset is 5 layers, and (c) EyePACS dataset is 16 layers.

DR, EyePACS datasets (5 classes each) are DeepPCANet-4, DeepPCANet-5, and DeepPCANet-16, respectively, and their specifications are shown in Figure 3. Each dataset is from different ethnicities; EyePACS dataset is from USA, APTOS2019 is from India, and KSU-DR is from KSA; as well as the use of different retinal images captured using different cameras so each dataset has different custom-designed model. After fixing the hyperparameters, each model is fine-tuned using training and validation sets for 100 epochs. The fine-tuned model is tested using the testing set.

## V. EXPERIMENTS AND RESULTS

This section first describes the evaluation protocol and the

experiments performed to evaluate the proposed method and then presents the results.

### A. Evaluation Protocol

We determined the architecture of the DeepPCANet for each DR dataset and fine-tuned it using the training set of the corresponding DR database; the detail is given in Section 3. After that, the performance of each model was evaluated using the test set of the related database. To validate the usefulness and the superiority of the model design technique, we compared custom-designed models with the widely used state-of-the-art pre-trained CNN models like ResNet [13], DenseNet [14], and ResNeSt [21], which have shown outstanding performance for

TABLE 2. COMPARISON BETWEEN DEEPPCANET MODELS AND THE PRETRAINED MODELS FOR SC1 SENARIO. G AND K STAND FOR GIGA AND K BYTES

Dataset	Model	#FLOPs	# parameters	ACC %	SE %	SP %	Kappa %
APTOS2019	ResNet152	5.6 G	60.19 G	95.25	88.22	96.97	88.15
	DensNet121	1.44 G	7.98 G	96.58	91.55	97.82	89.22
	ResNeSt50	5.39 G	27.5 G	97.11	92.29	98.2	90.82
	DeepPCANet-4	1.36 G	63.7 K	<b>98.21</b>	<b>95.29</b>	<b>98.9</b>	<b>94.32</b>
EyePACS	ResNet152			92.25	80.74	94.9	75.16
	DensNet121			91.14	80.07	95	74.84
	ResNeSt50			93.12	82.33	95.21	78
	DeepPCANet-16	2.11 G	557.68 K	<b>94.22</b>	<b>86.56</b>	<b>96.30</b>	<b>81.64</b>

TABLE 3. COMPARISON BETWEEN DEEPPCANET MODELS AND THE PRETRAINED MODELS FOR SC2 SENARIO

Dataset	Model	#FLOPs	# parameters	ACC %	SE %	SP %	Kappa %
KSU-DR dataset	ResNet152	5.6 G	60.19 G	97.98	97.83	97.83	95.75
	DenseNet121	1.44 G	7.98 G	98.51	96.06	98.86	96.4
	ResNeSt50	5.39 G	27.5 G	99.47	99.46	99.46	98.93
	DeepPCANet-5	1.375 G	73.66 K	<b>99.5</b>	<b>99.5</b>	<b>99.5</b>	<b>98.99</b>
APTOS2019	ResNet152			95	94.44	94.44	89.80
	DenseNet121			99.32	98.8	98.8	98.73
	ResNeSt50			98.33	96.54	96.53	94.22
	DeepPCANet-4	1.36 G	63.7 K	<b>99.7</b>	<b>99.44</b>	<b>99.44</b>	<b>99.3</b>
EyePACS	ResNet152			91.36	90.94	92.25	82.53
	DenseNet121			91.51	91.75	91.75	82.72
	ResNeSt50			90.53	90.92	90.92	79.04
	DeepPCANet-16	2.11 G	557.68 K	94.44	94.28	94.28	88.71

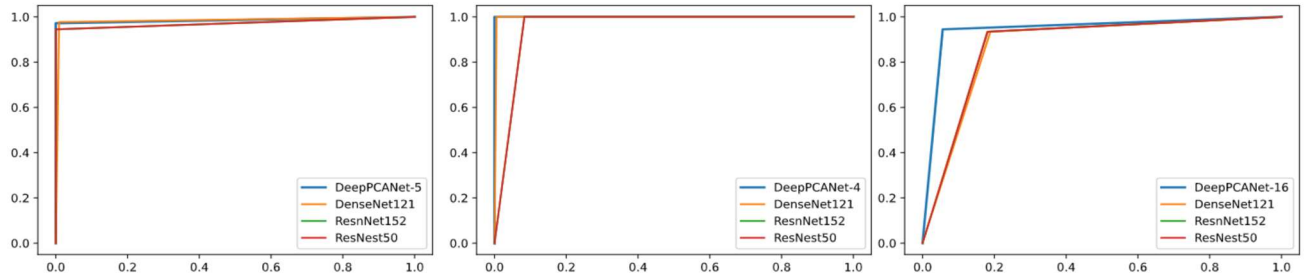


Fig. 5. ROC curve for custom-designed DeepPCANet and the pretrained models for SC2 senario and datasets: (a) KSU-DR, (b) APTOS-2019, (c) EyePACS

various computer vision applications. We fine-tuned the pre-trained models using the same procedure as was employed for DeepPCANet on each dataset.

For evaluation, we adopted three scenarios SC1 [29, 30], SC2 [28, 29], and SC3, as described in Section II.B. We evaluated the custom-designed models using SC1 and SC2 on APTOS2019 and EyePACS and SC3 in EyePACS. But evaluation on the KSU-DR dataset was done using SC2 because the number of images for five classes is not enough. In addition, we used four commonly used metrics in medical application and deep learning models: accuracy (ACC), sensitivity (SE), specificity (SP), and Kappa [11, 45-47].

### B. Five Class Problem (SC1)

Using the APTOS2019 and EyePACS datasets, we built DeepPCANet-4 and DeepPCANet-16 models, respectively, for SC1 using the respective training sets and fine-tuned them using the corresponding training and validation sets (see detail in Section 3). After fine-tuning, the models were evaluated on test datasets of EyePACS and APTOS2019; the results are shown in Table 2. The results of the ResNet152, DensNet121, and ResNeSt50 models, fine-tuned using the same training set and evaluated using the same testing set as for from EyePACS and APTOS2019, are also shown in Table 2. The results show that DeepPCANet-4 and DeepPCANet-16 outperform ResNet152, DensNet121, and ResNeSt50 on both datasets in terms of all metrics; in particular, in both cases, the sensitivity and Cohen's Kappa are higher than those of ResNet152, DensNet121, and ResNeSt50, Cohen's Kappa is considered more robust statistical measure than accuracy [48, 49]. The DeepPCANet-4 has the lowest number of FLOPs (1.36 G) and learnable parameters (63.7 K) among all competing models, as shown in Table 2. DeepPCANet-16 has fewer learnable parameters than the pertained ResNet152, DensNet121, and ResNeSt50 and also has less number of FLOPs than ResNet152 and ResNeSt50 models but slightly greater than DensNet121. In contrast, it has the best performance in terms of metrics on EyePACS dataset. ResNeSt50 has better performance than ResNet152 and DensNet121.

### C. Two Class Problem (SC2)

We validated the DeepPCANet models' performance using the three datasets for SC2. The custom-designed models DeepPCANet-5, DeepPCANet-4, and DeepPCANet-16 for KSU-DR, APTOS2019, and EyePACS, respectively, which were designed and fine-tuned using only fundus images, outperform the highly complex CNN models such as ResNet152, DensNet121, and ResNeSt50, which were trained using ImageNet dataset and fine-tuned using fundus images, in terms of all metrics, as shown in Table 3. Though DenseNet121 outperforms ResNet152 and ResNeSt50 on the three datasets, its performance is not better than the custom-designed models. DeepPCANet-5 involves 1.375G FLOPs, which is smaller than the number of FLOPs of ResNet152, DenseNet121, and ResNeSt50. The number of learnable parameters of DeepPCANet-5 is 73.66K which is much smaller than those of the pre-trained models ResNet152 (60.19 G),

DenseNet121 (7.98 G), and ResNeSt50(27.5 G). In Figure 5, we provide illustrations of the ROC curves on the three datasets using the four models (customized DeepPCANet, ResNet152, DenseNet121, and ResNeSt50). It indicates that DeepPCANet models' performance is better than the three pre-trained models on the three datasets.

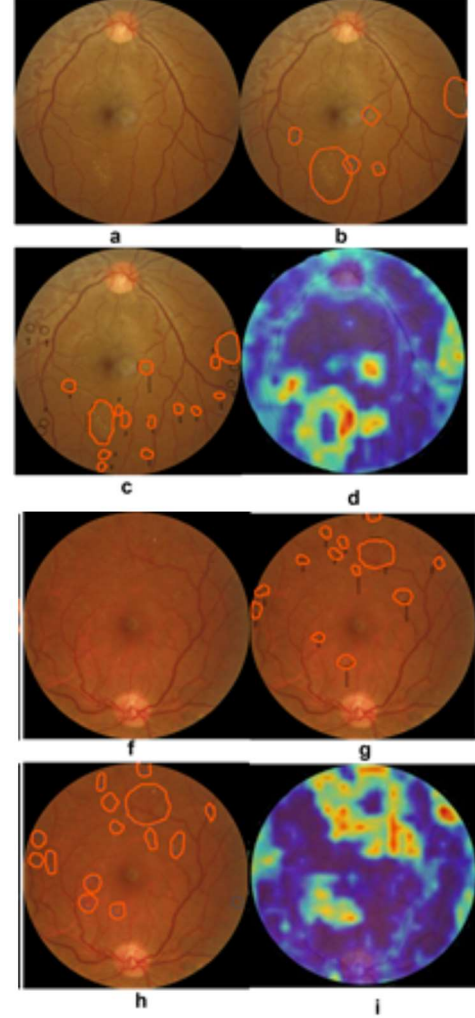


Fig. 6. Visualization of the decision making mechanism of DeepPCANet-5 model. (a) fundus image from class moderate, (b, c) lesions specified by experts 1 and 2, respectively, (d) DeepPCANet-5 map (f) fundus image from class pdf, (g,h) lesions specified by experts 1 and 2, respectively, (i) DeepPCANet-5 map.



#### D. Visualization

To understand the decision-making mechanism of the custom-designed CNN models, we created the visual feature maps using the gradient-weighted class activation mapping (GradCam) visualization method [50]. The visual feature maps of two random fundus images generated by the DeepPCANet-5 model customized for the local KSU-DR dataset are shown in Figures 5(d) and 5(i). The same fundus images were given blindly to two expert ophthalmologists at King Khalid Hospital of KSU, and they independently specified the lesion regions manually. Though there is a slight difference in the annotations of both experts, they agreed on most of the lesions, as shown in Figure 6 (b, c) for the fundus image (Figure 6a) from class moderate and Figure 6(g, h) for the fundus image (Figure 6f) from class pdf. The visual features maps of the DeepPCANet-5 model highlight the lesions annotated by both experts, as shown in Figure 5(d, i). The yellow and orange splatter in Figure.i

indicates that the DeepPCANet-5 model takes decisions based on the features learned from the lesion regions.

#### E. Discussions

This study proposed a technique to custom-design a DeepPCANet model for a target DR dataset. The depth of the model and the width of each layer is not specified randomly or by exhaustive experiments. The custom-designed DeepPCANet models for DR screening have small depths and varying widths of CONV layers and involve a small number of learnable parameters. The results of the DeepPCANet models customized for the KSU-DR, the APTOS2019, and the EyePACS datasets (presented in Tables 2 and 3), validate its superior performance against the famous highly complex pre-trained models ResNet152, DenseNet121, and ResNeSt50, which were fine-tuned using the same DR datasets. Generally, the DeepPCANet got competitive performance with a small number of layers and parameters. As shown in Table 3, the custom-designed

TABLE 4. COMPARISON BETWEEN DEEPPCANET MODELS AND STATE-OF-THE-ART METHODS

Paper	Method	Dataset	Performance (%)			
			ACC	SE	SP	Kappa
Five classes (SC1)						
Sikder et al. 2019 [32]	Colored features extraction using Ensemble	APTOS2019	91	89.54		
Tymchenko et al. 2020 [31]	An ensemble models with 3 CNN architectures ffcientNet-B4, EfficientNet-B5, and SE-ResNeXt50	APTOS2019	91.9	84	98	96.9
DeepPCANet-4	DeepPCANet model customized for APTOS2019 dataset	APTOS2019 (test: 40 % of public validation dataset)	98.21	95.28	98.85	94.32
Islam et al. 2018 [28]	A CNN model consisting of 18 layers with 3x3 and 4x4 kernels	EyePACS (test: 4% of dataset)		94.5	90.2	
Li et al. 2019 [29]	deep learning model based on DCNN	EyePACS (test: 10% of dataset)	86.17			
DeepPCANet-16	DeepPCANet model customized for EyePACS dataset	EyePACS (test: 10 % of public dataset)	94.22	86.56	96.30	81.64
Normal vs DR (all DR levels) (two classes) (SC2)						
Tymchenko et al. 2020 [31]	Ensembled models with 3 CNN architectures ffcientNet-B4, EfficientNet-B5, and SE-ResNeXt50	APTOS2019	99.3	99.3	99.3	98.6
DeepPCANet-4	DeepPCANet model customized for APTOS2019 dataset	APTOS2019(test: 10 % of public dataset)	99.7	99.44	99.44	99.3
Islam et al. 2018 [28]	A CNN model consisting of 18 layers with 3x3 and 4x4 kernels	EyePACS (test: 4% of public dataset)		94.5	90.2	
Li et al. 2019 [29]	Features extraction using deep learning model based on DCNN and SVM classification	EyePACS	91.05	89.30	90.89	
DeepPCANet-16	DeepPCANet model customized for EyePACS dataset	EyePACS (test: 10 % of public dataset)	94.44	94.28	94.28	88.71
Non-referral (Normal & DR grad 1) vs referral (DR grade 2 to highest grade) (two classes) (SC3)						
Colas et al. 2016 [33]	A CNN model. End to end training.	EyePACS (train:89%, test:11%)	96.2	66.6	94.6	
Islam et al. 2018 [28]	A CNN model	EyePACS (train:96%, test:4%)	98	94		
DeepPCANet-16	DeepPCANet model derived from EyePACS dataset	EyePACS (test: 10 % of public dataset)	94.59	94.86	94.87	89.02

DeepPCANet models for the three datasets have a small number of parameters in thousands against that number in millions of ResNet152, DensNet121, and ResNeSt50. DeepPCANet-4 and DeepPCANet-5 have fewer FLOPs than all pre-trained models and have better performance. The DeepPCANet-16 has fewer FLOPs than that of ResNet152 and ResNeSt50 and also has better performance. Though DensNet121 has fewer FLOPs than DeepPCANet-16, it has less performance and a large number of parameters. The reason for the lightweight structures and superior performance of custom-designed DeepPCANet models is that their architectures have been directly drawn from the fundus images, unlike the state-of-the-art CNN models, which have been mainly designed for object detection.

In addition to comparing the custom-designed DeepPCANet models with famous pre-trained models, it is essential to validate their effectiveness in DR screening by comparing them to the state-of-the-art methods on two challenging datasets (APTOS2019 and EyePACS). DeepPCANet-4 generated for SC1 on the APTOS2019 dataset outperforms the state-of-the-art methods on the same dataset in terms of accuracy, sensitivity, specificity, and Kappa, as shown in Table 4. Though the Method by Tymchenko et al. 2020 [31] outperforms the DeepPCANet-4 in the Kappa score for the five-class problem (SC1), it has less accuracy, sensitivity, specificity, and it is based on a highly complex ensemble of 20 CNN models. For the same scenario, the DeepPCANet-16 designed for EyePACS outperforms the existing methods in accuracy and specificity. The method by Islam et al. 2018 [28] got higher sensitivity, but their model is more complex, and it was tested on 4% of the dataset, as shown in Table 4.

For the SC2 (normal vs. DR levels), DeepPCANet-4 outperforms the method by Tymchenko et al. [31] in all metrics. In this scenario, on the EyePACS dataset, as shown Table 4, the DeepPCANet-16 is better than other methods in accuracy, sensitivity, and specificity; the method by Islam et al. 2018 [28] is slightly better than DeepPCANet-16 in sensitivity, but it was tested only on 4% of the EyePACS dataset.

The DeepPCANet-16, based on the EyePACS dataset for the SC3 (0 and 1 vs. DR levels), got less accuracy than Colas et al. [33] and Islam et al. [28] but got higher sensitivity and specificity, which are more important and robust than accuracy in the medical applications [51].

## VI. CONCLUSION

We introduced an approach to building a data-dependent CNN model – DeepPCANet - customized for DR screening automatically. This approach tackles the limitations of the available annotated DR datasets and the problem of a huge number of parameters in a deep CNN model. It builds a lightweight CNN model customized for a target DR dataset using k-medoid clustering, principal component analysis (PCA) and inter-class and intra-class variations. The DeepPCANet model is data-dependent, and each DR dataset has its appropriate architecture. The customized models, DeepPCANet-5 for the local KSU-DR dataset, DeepPCANet-4 for APTOS2019, and DeepPCANet-16 for EyePACS dataset, outperform the pre-trained very deep and highly complex

ResNet152, DenseNet121, and ResNeSt50 models fine-tuned using the same datasets and procedure. The performance, complexity, and number of parameters of the customized DeepPCANet models are less than ResNet152 and ResNeSt50 significantly. Though DensNet121 has fewer FLOPs than DeepPCANet-16, it has less performance and a large number of parameters. On the EyePACS dataset, compared to the state-of-the-art methods (for SC2 and SC3), the DeepPCANet-16 has less complexity and parameters and got a competitive performance. The DeepPCANet fails to predict DR grade from fundus images, which have poor quality. It could not grade some poor quality fundus images from the EyePACS dataset correctly; each image in this dataset was graded by only one expert from the geographic region of California, which can potentially lead to annotation bias. How the DeepPCANet can reliably predict the DR grade from poor quality fundus images is a subject of future work. Also, how the DeepPCANet can be generalized with different fundus datasets is a subject of future work.

## VII. REFERENCES

- [1] J. W. Yau, S. L. Rogers, R. Kawasaki *et al.*, "Global prevalence and major risk factors of diabetic retinopathy," *Diabetes care*, vol. 35, no. 3, pp. 556-564, 2012.
- [2] G. Quellec, K. Charrière, Y. Boudi *et al.*, "Deep image mining for diabetic retinopathy screening," *Medical Image Analysis*, 2017.
- [3] K. Sreejini, and V. Govindan, "Retrieval of pathological retina images using Bag of Visual Words and pLSA model," *Engineering Science and Technology, an International Journal*, vol. 22, no. 3, pp. 777-785, 2019.
- [4] D. J. Hemanth, O. Deperlioglu, and U. Kose, "An enhanced diabetic retinopathy detection and classification approach using deep convolutional neural network," *Neural Computing and Applications*, vol. 32, no. 3, pp. 707-721, 2020.
- [5] S. Stolte, and R. Fang, "A Survey on Medical Image Analysis in Diabetic Retinopathy," *Medical Image Analysis*, pp. 101742, 2020.
- [6] D. Ting, L. Pasquale, L. Peng *et al.*, "SW, Schmetterer, L., Keane, PA, & Wong, TY (2019)," *Artificial intelligence and deep learning in ophthalmology. British Journal of Ophthalmology*, vol. 103, no. 2, pp. 167-175.
- [7] J. Gu, Z. Wang, J. Kuen *et al.*, "Recent advances in convolutional neural networks," *Pattern Recognition*, vol. 77, pp. 354-377, 2018.
- [8] S. Grigorescu, B. Trasnea, T. Cocias *et al.*, "A survey of deep learning techniques for autonomous driving," *Journal of Field Robotics*, vol. 37, no. 3, pp. 362-386, 2020.
- [9] S. Abou Arkoub, A. H. El Hassani, F. Lauri *et al.*, "Survey on Deep Learning Techniques for Medical Imaging Application Area," *Machine Learning Paradigms*, pp. 149-189: Springer, 2020.
- [10] C. Lam, C. Yu, L. Huang *et al.*, "Retinal lesion detection with deep learning using image patches," *Investigative ophthalmology & visual science*, vol. 59, no. 1, pp. 590-596, 2018.
- [11] Z. Gao, J. Li, J. Guo *et al.*, "Diagnosis of Diabetic Retinopathy Using Deep Neural Networks," *IEEE Access*, vol. 7, pp. 3360-3370, 2019.
- [12] C. Szegedy, W. Liu, Y. Jia *et al.*, "Going deeper with convolutions." pp. 1-9.
- [13] K. He, X. Zhang, S. Ren *et al.*, "Deep residual learning for image recognition." pp. 770-778.
- [14] G. Huang, Z. Liu, K. Weinberger *et al.*, "Densely connected convolutional networks. CVPR 2017," *arXiv preprint arXiv:1608.06993*, 2016.
- [15] X. Glorot, and Y. Bengio, "Understanding the difficulty of training deep feedforward neural networks." pp. 249-256.
- [16] K. He, X. Zhang, S. Ren *et al.*, "Delving deep into rectifiers: Surpassing human-level performance on imagenet classification." pp. 1026-1034.
- [17] P. Krähenbühl, C. Doersch, J. Donahue *et al.*, "Data-dependent initializations of convolutional neural networks," *arXiv preprint arXiv:1511.06856*, 2015.

- [18] X. Suau, and N. Apostoloff, "Filter Distillation for Network Compression." pp. 3129-3138.
- [19] Kaggle. "Diabetic Retinopathy Detection (Kaggle)," 23-2, 2019; <https://www.kaggle.com/c/diabetic-retinopathy-detection/data>.
- [20] Kaggle. "APTOS blindness detection," 8-2020; <https://www.kaggle.com/c/aptos2019-blindness-detection>.
- [21] H. Zhang, C. Wu, Z. Zhang *et al.*, "Resnest: Split-attention networks," *arXiv preprint arXiv:2004.08955*, 2020.
- [22] M. Mateen, J. Wen, M. Hassan *et al.*, "Automatic Detection of Diabetic Retinopathy: A Review on Datasets, Methods and Evaluation Metrics," *IEEE Access*, vol. 8, pp. 48784-48811, 2020.
- [23] T. A. Soomro, A. J. Afifi, L. Zheng *et al.*, "Deep learning models for retinal blood vessels segmentation: A review," *IEEE Access*, vol. 7, pp. 71696-71717, 2019.
- [24] N. Asiri, M. Hussain, F. Al Adel *et al.*, "Deep learning based computer-aided diagnosis systems for diabetic retinopathy: A survey," *Artificial intelligence in medicine*, 2019.
- [25] T.-H. Chan, K. Jia, S. Gao *et al.*, "PCANet: A simple deep learning baseline for image classification?," *IEEE transactions on image processing*, vol. 24, no. 12, pp. 5017-5032, 2015.
- [26] M. Seuret, M. Alberti, M. Liwicki *et al.*, "PCA-initialized deep neural networks applied to document image analysis." pp. 877-882.
- [27] Z. Zhong, Z. Yang, B. Deng *et al.*, "Blockqnn: Efficient block-wise neural network architecture generation," *IEEE transactions on pattern analysis and machine intelligence*, 2020.
- [28] S. M. S. Islam, M. M. Hasan, and S. Abdullah, "Deep Learning based Early Detection and Grading of Diabetic Retinopathy Using Retinal Fundus Images," *arXiv preprint arXiv:1812.10595*, 2018.
- [29] Y.-H. Li, N.-N. Yeh, S.-J. Chen *et al.*, "Computer-assisted diagnosis for diabetic retinopathy based on fundus images using deep convolutional neural network," *Mobile Information Systems*, vol. 2019, 2019.
- [30] U. K. Challa, P. Yellamraju, and J. S. Bhatt, "A Multi-class Deep All-CNN for Detection of Diabetic Retinopathy Using Retinal Fundus Images." pp. 191-199.
- [31] B. Tymchenko, P. Marchenko, and D. Spodarets, "Deep Learning Approach to Diabetic Retinopathy Detection," *arXiv preprint arXiv:2003.02261*, 2020.
- [32] N. Sikder, M. S. Chowdhury, A. S. M. Arif *et al.*, "Early Blindness Detection Based on Retinal Images Using Ensemble Learning." pp. 1-6.
- [33] E. Colas, A. Besse, A. Orgogozo *et al.*, "Deep learning approach for diabetic retinopathy screening," *Acta Ophthalmologica*, vol. 94, 2016.
- [34] K. Simonyan, and A. Zisserman, "Very deep convolutional networks for large-scale image recognition," *arXiv preprint arXiv:1409.1556*, 2014.
- [35] J. Deng, W. Dong, R. Socher *et al.*, "Imagenet: A large-scale hierarchical image database." pp. 248-255.
- [36] Q. Zhang, and I. Couloigner, "A new and efficient k-medoid algorithm for spatial clustering." pp. 181-189.
- [37] S. Wold, K. Esbensen, and P. Geladi, "Principal component analysis," *Chemometrics and intelligent laboratory systems*, vol. 2, no. 1-3, pp. 37-52, 1987.
- [38] A. Likas, N. Vlassis, and J. J. Verbeek, "The global k-means clustering algorithm," *Pattern recognition*, vol. 36, no. 2, pp. 451-461, 2003.
- [39] F. R. "Saeed, SA), Hussain, Muhammed (Riyadh, SA), Aboalsamh, Hatim A. (Riyadh, SA)", *Method for fingerprint classification*, U. S. Paten, 2016.
- [40] R. Tibshirani, G. Walther, and T. Hastie, "Estimating the number of clusters in a data set via the gap statistic," *Journal of the Royal Statistical Society: Series B (Statistical Methodology)*, vol. 63, no. 2, pp. 411-423, 2001.
- [41] S. Mika, G. Ratsch, J. Weston *et al.*, "Fisher discriminant analysis with kernels." pp. 41-48.
- [42] A. A. M. H. Al Asbahi, F. Z. Gang, W. Iqbal *et al.*, "Novel approach of Principal Component Analysis method to assess the national energy performance via Energy Trilemma Index," *Energy Reports*, vol. 5, pp. 704-713, 2019.
- [43] A. Cook, "Global average pooling layers for object localization," *URL: [ht tps://alexisbcCook. github. io/2017-global-average-pooling-layers-for-object-localization](https://github.com/alexisbcCook/2017-global-average-pooling-layers-for-object-localization)* (Accessed on: 19. 08. 2019), 2017.
- [44] T. Akiba, S. Sano, T. Yanase *et al.*, "Optuna: A next-generation hyperparameter optimization framework." pp. 2623-2631.
- [45] G. Quellec, K. Charrière, Y. Boudi *et al.*, "Deep image mining for diabetic retinopathy screening," *Medical image analysis*, vol. 39, pp. 178-193, 2017.
- [46] A. R. Chowdhury, T. Chatterjee, and S. Banerjee, "A Random Forest classifier-based approach in the detection of abnormalities in the retina," *Medical & biological engineering & computing*, vol. 57, no. 1, pp. 193-203, 2019.
- [47] W. Zhang, J. Zhong, S. Yang *et al.*, "Automated identification and grading system of diabetic retinopathy using deep neural networks," *Knowledge-Based Systems*, 2019.
- [48] A. Ben-David, "Comparison of classification accuracy using Cohen's Weighted Kappa," *Expert Systems with Applications*, vol. 34, no. 2, pp. 825-832, 2008.
- [49] X. Fernández-Fuentes, D. Mera, A. Gómez *et al.*, "Towards a fast and accurate eit inverse problem solver: a machine learning approach," *Electronics*, vol. 7, no. 12, pp. 422, 2018.
- [50] R. R. Selvaraju, M. Cogswell, A. Das *et al.*, "Grad-cam: Visual explanations from deep networks via gradient-based localization." pp. 618-626.
- [51] C. R. Reynolds, and E. Fletcher-Janzen, "Handbook of clinical child neuropsychology," 2013.